CELL BIOLOGY

Light-induced dynamic structural color by intracellular 3D photonic crystals in brown algae

Martin Lopez-Garcia,[1,2] Nathan Masters,[3] Heath E. O'Brien,[3] Joseph Lennon,[4] George Atkinson,[4] Martin J. Cryan,[1] Ruth Oulton,[1,4] Heather M. Whitney[3]*

Natural photonic crystals are responsible for strong reflectance at selective wavelengths in different natural systems. We demonstrate that intracellular opal-like photonic crystals formed from lipids within photosynthetic cells produce vivid structural color in the alga *Cystoseira tamariscifolia*. The reflectance of the opaline vesicles is dynamically responsive to environmental illumination. The structural color is present in low light–adapted samples, whereas higher light levels produce a slow disappearance of the structural color such that it eventually vanishes completely. Once returned to low-light conditions, the color re-emerges. Our results suggest that these complex intracellular natural photonic crystals are responsive to environmental conditions, changing their packing structure reversibly, and have the potential to manipulate light for roles beyond visual signaling.

INTRODUCTION

Many organisms have evolved to make use of complex wavelength-scale geometries to manipulate light through optical interference (*1*). These structures are known as natural photonic crystals (PCs) (*2*) and present extraordinary optical properties for roles including color production and light harvesting (*3*). These structures are widespread in animals, for example, in insect cuticles and scales (*4*), feathers (*5*), and shells (*6*), and in most of the cases studied so far, they are predominantly extracellular. Structures range from one-dimensional (1D) layers (*7*) to full 3D structures (*8*) and, while usually static, can also be dynamic, for example, in chameleons (*9*). Plant photonic structures have been less well investigated. Most cases known are epicuticle or cellulose cell wall arrangements to form thin-layer or multifilm interference. There are examples of 1D PCs in plant cell walls (*10*) or within cells, which are composed of stacked membranes (*11*) or protein plates (*12*) that act as Bragg reflectors, but neither 3D intracellular PCs nor the type of changeable dynamic response observed in chameleons (*9*), cephalopods (*12*), or bacterial cultures (*13*) has ever been observed in complex photosynthetic organisms. Here, we describe an intracellular PC composed of spheres arranged in an opal-like PC (OPC) (*8*) structure and demonstrate that this structure produces the striking purple-to-green color in the brown alga *Cystoseira tamariscifolia*. This contradicts previous studies reporting that these bodies are composed of randomly scattered spheres (*14*). We also find this strong color to be reversibly dynamic, responding to light levels in the environment over a time scale of hours.

RESULTS AND DISCUSSION

C. tamariscifolia is a brown alga abundant on the Atlantic coast of Europe and the Mediterranean Sea (*15*) with vivid coloration (Fig. 1A). Despite a homogeneous coloration shown to the naked eye, inspection of the epidermal cells under low-magnification optical microscopy (Fig. 1, B to D) reveals "pointillist" coloration, with higher-magnification imaging showing highly reflective ≈5-μm-wide intracellular spherical vesicles that present colors ranging from deep blue to green (Fig. 1, E and F). The color within each vesicle is also not uniform, suggesting a complex inner structure. Hence, the structural color is not produced at the cuticle or cell wall of the epidermal cells as is known for other plants (*10*) and algae (*16*) but instead by intracellular bodies. Images taken in vivo of the epidermis in both reflectance and transmission configurations corroborate the position of the vesicle within the epidermal cells and reveal two to three vesicles per cell, with size varying between 2 and 5 μm (fig. S1). Cryo–scanning electron microscopy (SEM) and transmission electron microscopy (TEM) imaging (Fig. 2) show the OPCs surrounded by a cylindrical configuration of chloroplasts (see also fig. S2 and movie S1). Imaging using a selective fluorescent staining indicates that the vesicles' interior is mostly formed by lipids (Fig. 2D). X-ray spectroscopy also confirms (fig. S3) that the composition of the spheres is not formed of the most common materials found as main components of natural opals such as SiO_2 (*17*).

Electron microscopy reveals that the vesicles are filled with nanospheres organized in quasi–close-packed 3D lattice configurations very similar to those known in natural (*18*) and synthetic OPCs (Fig. 2) (*17*). The differences between our results and previous reports (*14*) are likely due to the use of freeze-fracture scanning (cryo-SEM) and freeze substitution TEM, which offer superior preservation of ultrastructure compared to the chemical fixation methods used in previous studies (*19*).

The highly ordered quasi–close-packed formation is conserved in all vesicles (Fig. 2, A and B). A statistical study of SEM and TEM images (fig. S3) indicates that each OPC is formed by quasi-monodisperse spherical bodies. That is, each OPC is formed by spheres of a given diameter ϕ. However, different OPCs will show different ϕ values that, as explained later, determine their optical properties. We have encountered values for ϕ varying from 150 to 250 nm on average between OPCs (fig. S3).

OPCs are commonly formed by close-packed monodisperse submicron spheres that assemble by natural (*18*) or artificial (*17*) methods to form a 3D lattice. The optical properties of the structure will then be dependent on the size and the arrangement of the spheres and on the materials forming the opal. The best-known consequence of these periodic arrangements of spheres is the creation of a bright reflectance with strong wavelength and directional dependency due to constructive/destructive interference of light within the structure. In natural or synthetic opals, the most common lattice type in which the spheres might arrange is the face-centered cubic (FCC) (*8*). We can

[1]Department of Electrical and Electronic Engineering, University of Bristol, Bristol BS8 1TH, UK. [2]Department of Nanophotonics, International Iberian Nanotechnology Laboratory, 4715-330 Braga, Portugal. [3]School of Biological Sciences, University of Bristol, Life Sciences Building, 24 Tyndall Avenue, Bristol BS8 1TQ, UK. [4]School of Physics, Henry Herbert Wills Physics Laboratory, University of Bristol, Tyndall Avenue, Bristol BS8 1TL, UK.
*Corresponding author. Email: heather.whitney@bristol.ac.uk

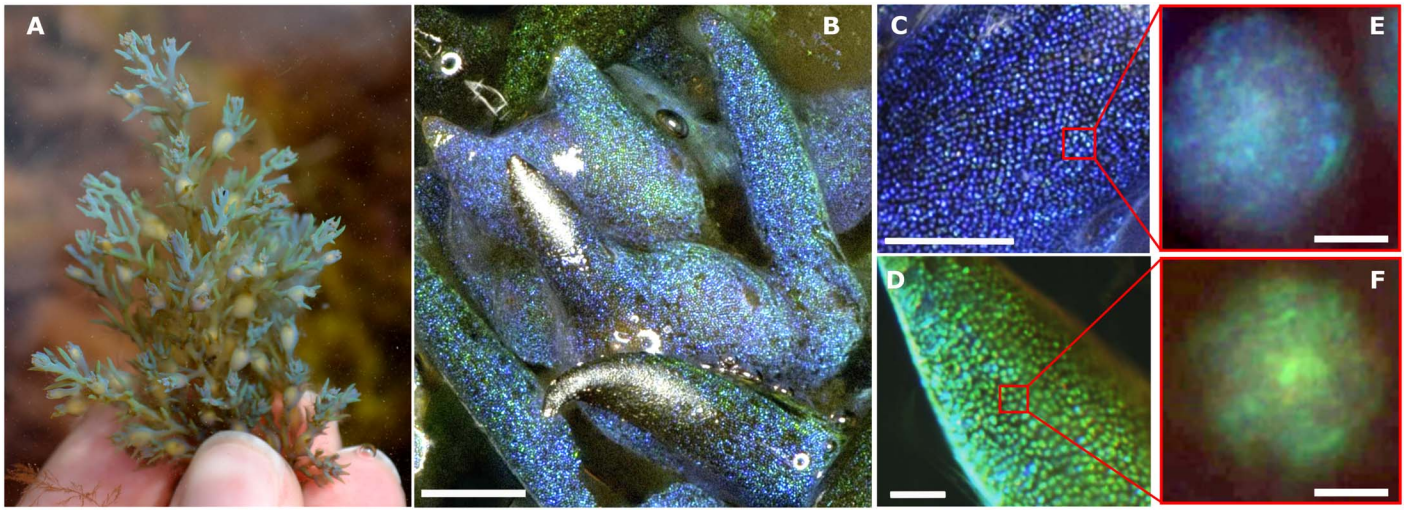

Fig. 1. Morphology and structural color of *C. tamariscifolia*. (**A**) *C. tamariscifolia* at collection site showing structural color. (**B**) Low-magnification (scale bar, 500 μm) image of a specimen with two different colors. Close-up of tips of blue (**C**) and green (**D**) specimens. Scale bars, 50 μm. (**E** and **F**) Single vesicles in the epidermal cells of two different specimens under a high-magnification optical microscope. Scale bars, 2 μm).

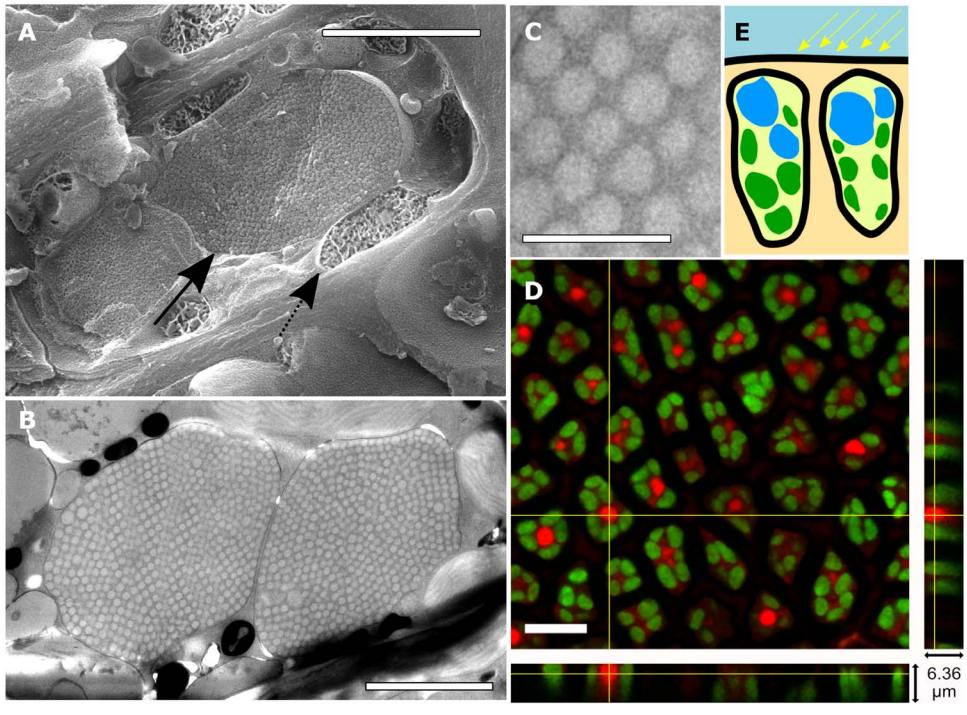

Fig. 2. Structure and composition of OPCs. (**A**) Cryo-SEM image of an epidermal cell. Scale bar, 2 μm. Arrows indicate OPC (solid) and chloroplast (dashed) positions within the cell. (**B**) Cross section of a single epidermal cell (TEM image). Scale bar, 2.5 μm. (**C**) Nanospheres in quasi–close-packed configuration. Scale bar, 1 μm. (**D**) False-color fluorescence confocal images of epidermal cells for chlorophyll (green) and Nile red lipophilic dye (red). Scale bar, 10 μm. (**E**) Sketch of position for OPCs (blue) and chloroplast (green) within the epidermal cells.

gain an understanding of the underlying structure of the opals by using well-known optical characterization techniques: Information about the sphere size, lattice type, refractive index of the sphere, and the surroundings allow us to analytically confirm the opalescent nature. In particular, measurements of the spectral angular dependence allow us to confirm conclusively that the optical properties arise from interference effects.

To characterize the optical properties of the natural OPC, we performed in vivo spectroscopy and scatterometry (see Materials and Methods) over single cells using Fourier image spectroscopy (*20*). Figure 3A shows three spectra taken over different cells in vivo. A strong peak in normal-incidence reflectance is measured for wavelengths matching the colors recorded under an optical microscope. According to our observations, the maximum reflectance occurs for a central wavelength (λ_c) that can range from $\lambda_c \approx 440$ to 550 nm depending on the cell inspected. The maximum reflectance (R) for a single OPC varies between 5 and 10% with values obtained after normalization by the reflectance of a silver

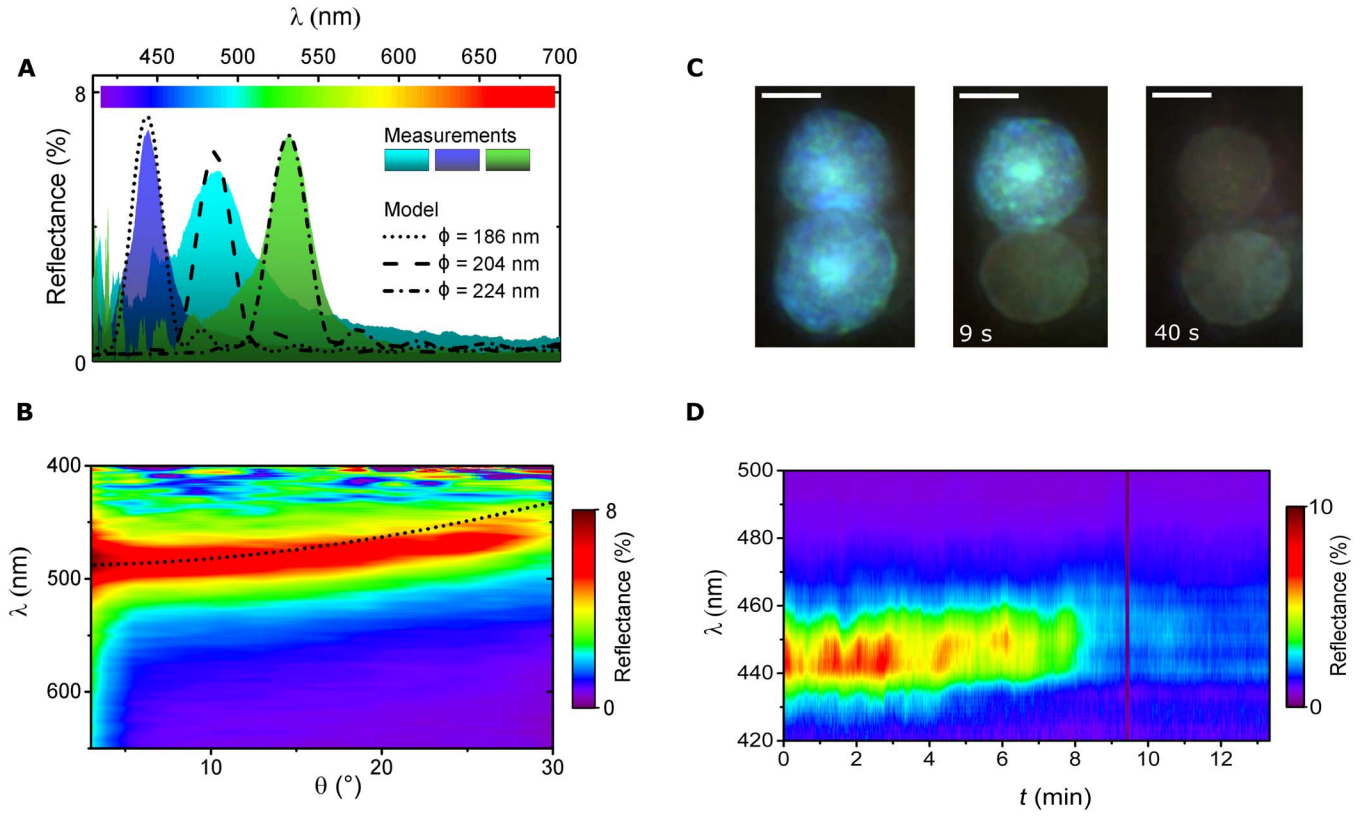

Fig. 3. Optical properties of OPCs. (**A**) In vivo normal-incidence reflectance measurements for three different OPCs (filled curves). Single-line curves correspond to simulations for an FCC lattice of spheres with ϕ = 186 (dotted), 204 (dashed), and 224 nm (dotted-dashed line). In all cases, n_{sph} = 1.48 and n_{cyt} = 1.35. The number of monolayers forming the opal was N = 18 (dotted and dash-dotted) and N = 17 (dashed). (**B**) Angular reflectance measurements for a single OPC. The dotted line shows calculation for the central reflectance wavelength of an opal using effective refractive index approximation ϕ = 200 nm. (**C**) Single-cell structural color decay under continuous local illumination. Images extracted from movie S2 at times 0, 9, and 40 s. Scale bars, 3 μm. (**D**) Reflectance decay of a single OPC under continuous illumination.

mirror. Reflectance as high as 10% shows that optical performance of the OPCs is comparable to that of other iridescent photosynthetic systems (*3*, *21*).

Because our experiments support the PC nature of the OPCs, a model of the whole natural photonic system was constructed. We considered each single OPC as an FCC lattice formed by monodisperse spheres of diameter ϕ and refractive index n_{sph} and where the structure is formed by N monolayers of spheres that combine to form the 3D lattice (fig. S5). Because the refractive index for biological lipids and surrounding aqueous cytoplasm (n_{cyt}) has been established (*22*), we considered that n_{sph} = 1.48 and n_{cyt} = 1.35. Measured reflectance values of several OPCs correspond very closely to simulation results when ϕ is set to values within the range of observed diameters (Fig. 3A). We found good agreement for ϕ = 186, 204, and 224 nm in the case of the three reflectance peaks in Fig. 3. The number of monolayers N varies between N = 15 and 20 stacks from edge to edge of the vesicle. These values are also consistent with the inspection of the freeze-fracture TEM images such as those shown in Fig. 2B. Note that some polydispersity of the spheres and small local variations in n_{sph} are to be expected in the real OPC. The former could be the cause for the heterogeneous coloration of the natural OPCs, whereas the latter is known to account for spectral broadening and reflectance reduction (*17*).

We further test our model by performing angular reflectance measurements over single cells. Figure 3B shows the angular reflectance of a single vesicle under omnidirectional illumination (*23*). As observed in Fig. 3B, a blue shift of the reflectance occurs as the collection angle increases. This is a characteristic feature of opal structures (*24*). The central wavelength of the reflectivity peak, λ_c, for a given incidence angle can be calculated by approximating the structure as a multilayer with an effective refractive index dependent on the orientation of the FCC lattice (fig. S5) (*25*). The dotted line in Fig. 3B shows the result of using this approximation for an FCC lattice of close-packed spheres with n_{cyt} = 1.35, n_{sph} = 1.48, and ϕ = 200 nm. The agreement is good but with a slightly higher blue shift at large angles for the theoretical value. This can be attributed to lattice disorder and to the spherical shape of the vesicle, which affects the incident angle (*10*).

The OPCs found in *C. tamariscifolia* therefore have the potential to interact with and modify light levels within photosynthetic cells. The intertidal zone where *C. tamariscifolia* grows is a particularly challenging light environment because of extreme fluctuations in light levels at low and high tides (fig. S6, A to C). We investigated whether OPCs could play a role in adaptation to variable light levels by subjecting living samples of *C. tamariscifolia* to dark and light conditions while color was monitored.

We inspected light-induced changes in structural color at single-OPC level under the microscope. As shown in Fig. 3 (C and D), the optics of single OPCs was observed to change from a steady reflectance in dark conditions ($R \approx 10\%$) to no reflectance ($R < 5\%$) after high-intensity

illumination with white light with an intensity of 10^4 µmol/m^2s for ≈10 min. However, once an OPC begins to fade, the transition often takes place in less than 2 s (movie S2 and fig. S6D). The structural color of OPCs decays at different times for the same illumination area, even within the same cell (Fig. 3C), where the color of the lower OPC vanished by 9 s, whereas the upper one remains highly reflective, fading by 40 s of illumination. However, our preliminary observations suggest a cross-talk mechanism between neighboring vesicles in the same cell by which the discoloration happens within the same time interval for the whole area of illumination (movie S3).

Illumination under the microscope is far more intense than in the natural environment, so to mimic field conditions, the dynamic structural color was also monitored across several entire specimens (Fig. 4, A and B). All of the specimens were kept at controlled conditions in an aquarium under photosynthetic active radiation (PAR) light intensities (61.2 µmol/m^2s) and water temperature (≈14°C) biologically relevant to mimic field conditions (fig. S6) (*26*). Illumination was switched ON/OFF with different cycle durations (to confound any circadian effects) while changes in structural color were monitored by taking images of the specimen every 20 min. Iridescence is observable under dark conditions [dark conformation (DC)]. When illuminated [light conformation (LC)], the color fades in a time scale of 2 to 3 hours for the whole specimen. The low iridescence in LC remains constant (Fig. 4C) until dark conditions are restored, with iridescence being recovered after the specimen is set in the dark for 2 to 3 hours. Varying the LC/DC cycles confirms that the structural color decay/emergence is repeatable and occurs on a 2- to 3-hour time scale independent of the length of the cycles (fig. S7). This supports the hypothesis that external-light levels trigger the dynamic changes in reflectance rather than being a response to an internal circadian rhythm.

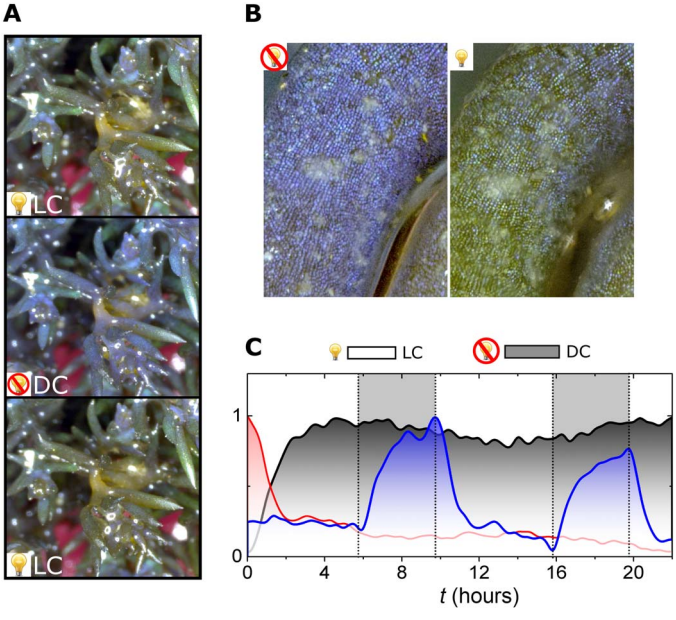

Fig. 4. Light-induced iridescence dynamics. (**A**) Stereomicrograph of *C. tamariscifolia* specimen in LC (top), after 12 hours in DC (middle), and return to LC (bottom) after illumination for 12 hours. (**B**) Details of the same specimen in (A) for DC (left) and LC (right) with dark/light adaptation periods of 12 hours, respectively. (**C**) Evolution of structural color intensity (I_B/I_{RGB}) during illumination and dark periods. Red and gray lines show continuous light and dark adaptation, respectively, for 24 hours. The solid blue line shows structural color for an illumination pattern with a duty cycle of LC 6 hours/DC 4 hours during 24 hours. Gray areas delimited by dotted lines highlight times where the illumination lamp is ON to trigger LC.

We now consider the potential mechanisms that may account for the rapid change in color of a single OPC. Light microscopy (Fig. 3C and movies S2 and S4) shows that the decay of the structural color is neither due to a rupture of the OPC vesicles nor can cytoplasm refractive index changes account for the disappearance of reflectance (see simulations in fig. S8).

By measuring the relative position of the spheres in TEM images (see Materials and Methods and fig. S9) for LC and DC specimens (Fig. 5A), we find that there is an expansion of the distance (*d*) between spheres in LC compared to DC specimens (Fig. 5B). Moreover, 2D Fourier power spectra (*27*) of the same TEM images (fig. S9B) show that DC (blue) specimens present a strong peak for a center-to-center distance of ≈170 nm (0.006 nm^{-1}) between lipid spheres. The same analysis over LC (brown) specimens shows no prevalence of any center-to-center distance (fig. S9B), suggesting that the expansion of the lattice is encompassed by a randomization of the positions for each sphere.

Calculations of the reflectance as a function of the lattice expansion of the OPCs (Fig. 5C) show that an expansion of the lattice will produce a red shift of the central wavelength of the reflectance peak. The calculated absolute reflectance is not reduced but rather slightly increased by the expansion of the lattice. This increase in reflectance is not observed in our experiments, where a quick decay of the reflectance is observed under certain light conditions, as shown in Fig. 4. To find the reason for this discrepancy, we calculated the reflectance of a random distribution of spheres of the same diameter (Fig. 5C, blue-shadowed area). As can be observed, the characteristic reflectance peak of the OPC vanishes completely for randomly positioned spheres. Hence, combining the optical model with the Fourier power spectral analysis over the TEM images suggests that the possible mechanism of structural color reduction might be a combination of expansion and randomization of the lattice. During the first stage of expansion, the lattice would still be relatively ordered, leading to a red shift of the reflectance. However, after the initial expansion, the spheres would be free to move within the vesicle, and a randomization of their position is then possible, producing the reflectance to vanish. The vanishing of structural color is preceded by a red shift from blue to green (movie S4), supporting the idea of a combined expansion-randomization of the lattice.

The formation of an opaline structure from lipid microspheres is, as far as we are aware, unique to both the natural world and synthetic opals. The fact that the alga is able to form monodisperse spheres and control their packing structure is by itself surprising, but the fact that the alga is able to precisely change the packing structure from ordered to disordered, and in a reversible manner, is remarkable.

The function of the OPCs for the alga also remains to be determined, but the position of the OPCs relative to the chloroplasts in the cell, together with the dynamics of the photonic properties, strongly indicates a photosynthetic role. The chloroplasts are oriented with their long axes parallel to the direction of incident light (see fig. S10), reducing the surface area exposed to light transmitted directly from the thallus surface (*28*). It is well documented that chloroplasts in many other shade-adapted plants move to the periphery of the cell when exposed to high-light conditions to minimize light exposure (*29*). However, we believe that, in this alga, the chloroplasts may remain more static, with the OPC regulating the exposure of the chloroplasts to light instead.

We propose that it is the photonic "stopband" (the spectral region over which the OPC is highly reflective) that regulates the light reaching

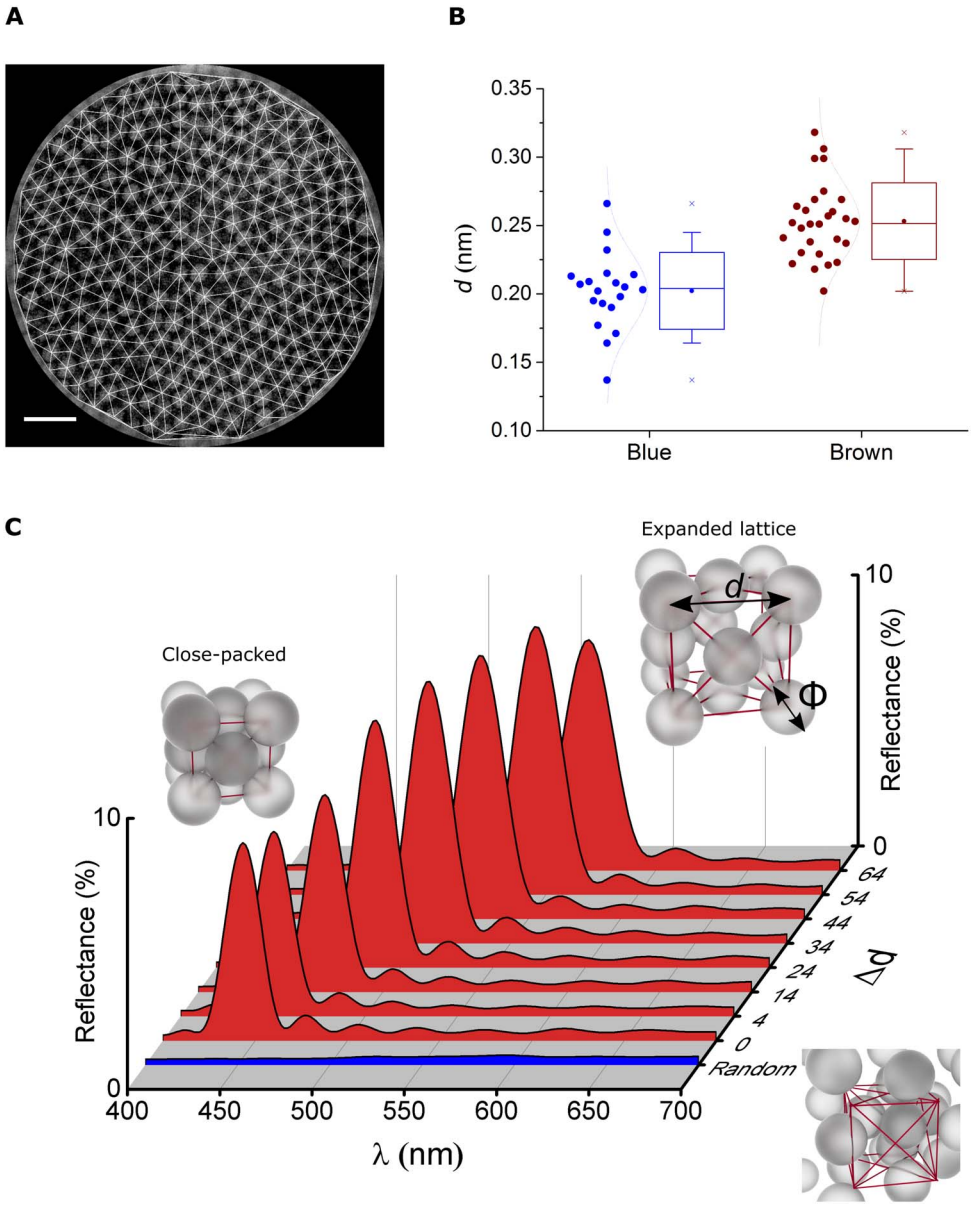

Fig. 5. Structural color decay by lattice expansion. (**A**) TEM images of a single vesicle used to study the lattice expansion under different conditions. (**B**) Statistical analysis (see fig. S9) of the distance between particles forming the OPCs for brown (LC) and blue (DC). Data suggest an expansion of the lattice for brown specimens. (**C**) Simulations of reflectance of an FCC lattice of spheres under different lattice expansions. d is the lattice parameter and Δd the lattice parameter expansion ($d = d_o + \Delta d$). $d_o = \sqrt{2}\phi$, the case for which the spheres with diameter ϕ are close-packed. The blue-shadowed area shows reflectance calculated for a random distribution of the same spheres. All other parameters in the simulation are the same used in Fig. 3A.

the chloroplasts. When in their disordered state (during the LC phase), the stopband is not present, and the vesicle transmits the light in a similar way to any other region of the cell. This configuration is shown in fig. S10A, where one can see that the light is transmitted through the vesicle, with minimal interaction with the chloroplasts. However, in the DC phase, the lipid spheres in the vesicle become ordered into an OPC. A stopband forms, and the surface of the spherical structure becomes highly reflective. This configuration is shown in fig. S10B. Although some of the light is scattered back out of the top (this is, what is observed in optical microscopy as the bright blue reflection), the spherical shape means that light is also scattered toward the sides. This ensures that less light is transmitted and that more light is scattered toward the chloroplasts in low-light conditions. Thus, in bright light, the OPC is inactive and the chloroplasts are protected by aligning themselves to minimize their cross section with light as a photoprotective mechanism, whereas when little light is available, the OPC becomes ordered to ensure that it scatters light to ensure maximum exposure to the chloroplasts.

Note that this configuration acts in a somewhat different way from the mechanism proposed for the only other aquatic photosynthetic system to report photonic structures believed to enhance photosynthesis (*30*). In this complex symbiotic system inside a clam, transmissive Bragg reflectors selectively transmit the desired wavelengths to deep within the tissue. In the case of the alga here, it is the highly reflective property of the OPC that is used.

CONCLUSIONS

The extraordinary capacity of PCs to efficiently modulate light-matter interaction is well known in solar cell photovoltaics (*31*) and natural photonic structures (*2*). Very recently, two other examples of PCs with a role in light harvesting for photosynthesis have been documented, having evolved separately (*3*, *30*). However, all previous examples of photonic structures in plants are of 1D structures. Here, we report a complex 3D opal structure formed from lipids.

The presence of such a complex photonic structure in an alga, such as the ordered 3D opal structure shown here, is surprising in itself but even more so is the fact that this complex structure is dynamic. How the alga is able to produce quasi-monodisperse lipids and control the level of order or disorder, reversibly, remains unknown, but it certainly surpasses the capabilities of current artificial opal synthesis. The biological function of this opal is also unknown, but its location close to chloroplasts hints at a complex interplay between the photonic structure and photosynthesis. Note that, although other PCs found in other species of algae are thought to have a photoprotection function (*21*), we hypothesize that, because the OPC is active in low-light conditions, its role is to scatter light efficiently in low-light conditions to the chloroplasts, which are otherwise in a photoprotective alignment. This adaptation appears to be a response to the extreme variation in light conditions in which this intertidal alga is found. Our results are consistent with the possibility that photosynthetic organisms can use physical photonic structures to manipulate photosynthesis beyond the photochemical process.

MATERIALS AND METHODS

Specimen collection and field study

Specimens of *C. tamariscifolia* were collected from rock pools on the southwest coast of the UK and maintained for up to 2 months in natural seawater in commercial aquaria with carbon/zeolite filtration (Marina 360 Degree Aquarium, Hagen) at 14°C. The illumination was provided by fluorescent tubes (GE Lighting F15W/35-535) with a biologically relevant spectral and intensity specifications (see details about illumination in figs. S6 and S7).

Photographs in Fig. 1 were taken using a Nikon D3200 photographic camera. Low-magnification microscopy in Figs. 1 and 4 used a VHX-1000E Digital Microscope (Keyence) with a polarizing filter.

PAR in the aquaria and in the field was measured with a calibrated LI-COR Quantum Sensor (LI-250A). In-field measurements of PAR were performed by placing the PAR meter next to the specimens during rising/falling tide.

In vivo PC optical property characterization

For high-resolution optical characterization, we used a custom-made white-light epi-illumination reflectance microscope. White-light lamp illumination (Thorlabs OSL-1) was collimated and focused on the sample with a high numerical aperture (0.75) objective lens (Zeiss 63X). This illumination configuration mimics light conditions in the natural environment of the alga where light is incident on the specimen with no preferential direction. The collected light was then focused onto an optical fiber (Thorlabs M92L01) in a confocal configuration. A modified configuration of the previous setup allowed Fourier image spectroscopy over the whole numerical aperture of the objective lens. This technique allows the measurement of reflectance (R) as a function of collection angle and is a typical method used to characterize PCs. The lateral size of the illumination spot is approximately 8 μm, enough to resolve reflectance of single cells on one measurement.

Cell and OPC morphological characterization

For TEM, apical tips approximately 1 to 2 mm in length were frozen in an EM PACT2 high-pressure freezer (Leica Microsystems) in 0.2-mm gold-coated live-cell carriers using seawater as a cryopreservative. Specimens were put in 1% osmium tetroxide and 0.1% uranyl acetate in anhydrous acetone at −90°C and transferred to an EM AFS1 Leica Microsystems freeze substitution apparatus where they were left at −90°C for 5 hours, before the temperature was decreased from 5°C/hour to 0°C/hour. Samples were washed twice with cold acetone and gradually infiltrated with increasing ratios of acetone/Epon (3:1, 1:1, and 1:3) for 1 hour each step followed by 2 hours in pure Epon. Samples were hardened overnight at 60°C, and then, 70-nm sections were cut using an Ultracut 7 ultramicrotome (Leica Microsystems), mounted on Pioloform-coated copper grids, and stained with 1 to 3% uranyl acetate followed by lead citrate staining. Stained sections were viewed with a Tecnai T12 TEM (FEI). For freeze-fracture SEM (cryo-SEM), samples were frozen by plunging them into a liquid nitrogen slush and then fractured with a scalpel blade. Samples were sputter-coated with platinum and then imaged using a Quanta 400 Tungsten scanning electron microscope. Energy-dispersive spectroscopy was carried out using an X-Max Detector (Oxford Instruments) attached to a Hitachi SU8230 Cold Field Emission scanning electron microscope. This test (fig. S4) was necessary to corroborate that the nanospheres forming the OPC were not constituted by material known to for other artificial opals in nature such as SiO_2.

The central position of each nanosphere was identified on a set of TEM images for both light-adapted (brown) and dark-adapted (blue) specimens (see fig. S10), and the distance (d) to adjacent nanospheres was calculated using a Delaunay triangulation method. Fourier power spectra for center-to-center frequency evaluation were obtained by fast Fourier transform of TEM images using ImageJ software.

Confocal microscopy was performed on a Leica DMI 6000 CS inverted confocal microscope with a 100× oil immersion objective. Chloroplast autofluorescence was imaged with an excitation beam of 488 nm and emission measured over a wavelength range of 650 to 750 nm. Z-step size was 0.165 μm and controlled through Leica AF software. Samples were prepared by a single slice along the length of the specimen, and the epidermal tissue was imaged. For lipophilic staining, a Nile red stain (N3013, Sigma-Aldrich) was used. Fresh cuts were taken without fixing before being stained at a concentration of 10 μl/ml for 1 hour, followed by three washes. Stained samples were imaged by confocal microscopy as described above, with excitation at 488 nm and emission measured over a range of 575 to 625 nm. A Z-step size of 0.30 μm was used.

High-resolution images for the iridescence dynamics study over whole specimens were obtained with a GoPro HERO4 complementary metal-oxide semiconductor camera. Illumination by the fluorescent tubes of the aquarium was synchronized with the camera through a python programming language home-made driver controlled by a Raspberry Pi Model B unit. Images were taken every 20 min, and storage for further analysis was done using an ImageJ software. The normalized intensity recorded in the blue channel of the camera divided by the total intensity (calculated as the sum of all channels) gives the normalized intensity (I_B/I_{RGB}) of the structural color on each image and was evaluated over relevant areas of the image by obtaining the ratio between the intensities collected in the blue channel. To take images during DC, the fluorescent tubes were switched off and only switched on for 4 s every 20 s to record the image.

Optical model: Full-structure simulation

As an optical model, we constructed each single OPC as an FCC lattice formed by monodisperse spheres of diameter ϕ and refractive index n_{sph} oriented normal to the surface along the ΓL crystallographic direction (d_{111} crystallographic plane). Values for ϕ included in the model were chosen within the range obtained from the TEM/SEM images. The whole structure was considered to be immersed in a homogeneous medium with refractive index n_{cyt}. To make model and experiments comparable, it is fair to expect that OPCs in different cells will present differences in the number of layers of spheres and their diameter, as well as small variances in n_{cyt} and n_{sph}. Using values reported in literature (*23*), we considered cytoplasm ($n_{cyt} = 1.35$) as the medium in which the spheres are immersed within the vesicles and $n_{sph} = 1.48$ as the refractive index of the lipid nanospheres.

Changes in refractive index for any of the two parts of the structure [spheres and immersion medium (cytoplasm)] have two effects. One effect is that, reflectance can be enhanced (decreased) if refractive index contrast is increased (reduced). The other important effect is an overall red shift for larger refractive indices. Note that a third effect of increasing the refractive index contrast is spectral broadening of the reflecting peak. However, for small refractive index contrast ($n_{sph} \approx n_{cyt}$), little broadening is expected.

Optical model: Bragg stack approximation

For calculation of the angular dependency of the reflectance peak, we used the well-established Bragg stack approximation for opals (*31*). Each set of spheres in the same plane of crystal growth is averaged by a given effective refractive index ($\bar{n}$). The destructive interference of an incident beam within the crystal is fulfilled for $\lambda_c = 2d_{xyz}\sqrt{\bar{n}^2 - \sin^2\theta}$, where λ_c is the central wavelength for the resulting reflectance peak, d_{xyz} is the crystallographic plane of the opal, and θ is the angle of incidence/collection considered. We considered here the opal to be oriented with its Γ-L direction toward the surface of the alga, and therefore, plane d_{111} should be used (fig. S5). In the case of close-packed spheres, $d_{111} = \sqrt{2/3}\,\phi$, with ϕ being the diameter of the spheres. $\bar{n}$ is calculated as $\bar{n} = \sqrt{f n_{sph}^2 + (1-f) n_{cyt}^2}$, where f is the filling fraction of spheres, that is, the volume filled by spheres in the total volume occupied by the PC. n_{sph} and n_{cyt} are the refractive index for the spheres and the surrounding medium (cytoplasm), respectively. For a close-packed opal PC, $f = 0.74$.

SUPPLEMENTARY MATERIALS

Supplementary material for this article is available at http://advances.sciencemag.org/cgi/content/full/4/4/eaan8917/DC1

fig. S1. High-magnification in vivo optical microscopy (115×) images of the epidermal region.
fig. S2. Position of the OPCs and chloroplast in the epidermal cells.
fig. S3. Energy-dispersive x-ray analysis over several epidermal cells containing OPCs.
fig. S4. Statistical analysis of single OPC properties.
fig. S5. Arrangement of the spheres within the OPCs.
fig. S6. Relevant spectra and intensities for the light sources used in the experiments.
fig. S7. Dynamics of structural color.
fig. S8. Calculated reflectance of an OPC as a function of cytoplasm refractive index.
fig. S9. Statistical analysis of lattice expansion on OPCs between dark and light conformation.
fig. S10. Sketches of possible mechanism for light flux redirectioning into the chloroplast.
movie S1. Three-dimensional autofluorescence confocal false-color maps showing the relative position between OPCs (red) and chloroplasts (green) within the epidermal cells.
movie S2. Structural color decay for the two OPCs shown in Fig. 3C.
movie S3. Structural color decay filmed with stereomicroscope under low magnification.
movie S4. Fast decay of structural color for OPCs under continuous illumination.

REFERENCES AND NOTES

1. S. Kinoshita, S. Yoshioka, J. Miyazaki, Physics of structural colors. *Rep. Prog. Phys.* **71**, 076401 (2008).
2. P. Vukusic, J. R. Sambles, Photonic structures in biology. *Nature* **424**, 852–855 (2003).
3. M. Jacobs, M. Lopez-Garcia, O.-P. Phrathep, T. Lawson, R. Oulton, H. M. Whitney, Photonic multilayer structure of *Begonia* chloroplasts enhances photosynthetic efficiency. *Nat. Plants* **2**, 16162 (2016).
4. P. Simonis, J. P. Vigneron, Structural color produced by a three-dimensional photonic polycrystal in the scales of a longhorn beetle: *Pseudomyagrus waterhousei* (Coleoptera: Cerambicidae). *Phys. Rev. E* **83**, 011908 (2011).
5. J. P. Vigneron, J.-F. Colomer, M. Rassart, A. L. Ingram, V. Lousse, Structural origin of the colored reflections from the black-billed magpie feathers. *Phys. Rev. E* **73**, 021914 (2006).
6. L. Li, S. Kolle, J. C. Weaver, C. Ortiz, J. Aizenberg, M. Kolle, A highly conspicuous mineralized composite photonic architecture in the translucent shell of the blue-rayed limpet. *Nat. Commun.* **6**, 6322 (2015).
7. P. Vukusic, J. R. Sambles, C. R. Lawrence, Colour mixing in wing scales of a butterfly. *Nature* **404**, 457 (2000).
8. A. R. Parker, V. L. Welch, D. Driver, N. Martini, Structural colour: Opal analogue discovered in a weevil. *Nature* **426**, 786–787 (2003).
9. J. Teyssier, S. V. Saenko, D. van der Marel, M. C. Milinkovitch, Photonic crystals cause active colour change in chameleons. *Nat. Commun.* **6**, 6368 (2015).
10. S. Vignolini, P. J. Rudall, A. V. Rowland, A. Reed, E. Moyroud, R. B. Faden, J. J. Baumberg, B. J. Glover, U. Steiner, Pointillist structural color in *Pollia* fruit. *Proc. Natl. Acad. Sci. U.S.A.* **109**, 15712–15715 (2012).
11. D. W. Lee, J. B. Lowry, Physical basis and ecological significance of iridescence in blue plants. *Nature* **254**, 50–51 (1975).
12. A. L. Holt, A. M. Sweeney, S. Johnsen, D. E. Morse, A highly distributed Bragg stack with unique geometry provides effective camouflage for Loliginid squid eyes. *J. R. Soc. Interface* **8**, 1386–1399 (2011).
13. B. Kientz, P. Vukusic, S. Luke, E. Rosenfeld, Iridescence of a marine bacterium and classification of prokaryotic structural colors. *Appl. Environ. Microbiol.* **78**, 2092–2099 (2012).
14. L. Pellegrini, M. Pellegrini, Iridescent bodies of *Cystoseira stricta* Sauvageau (Phaeophyta, Fucales): Their fine structure, development and nature in vegetative cells. *Phycologia* **21**, 34–46 (1982).
15. W. D. P. Steward, Occurrence of *Cystoseira tamariscifolia* (Huds.) Papenf. on the West Coast of Scotland. *Nature* **195**, 402–403 (1962).
16. W. H. Gerwick, N. J. Lang, Structural, chemical and ecological studies on iridescence in *Iridaea* (Rhodophyta). *J. Phycol.* **13**, 121–127 (1977).
17. J. F. Galisteo-López, M. Ibisate, R. Sapienza, L. S. Froufe-Pérez, Á. Blanco, C. López, Self-assembled photonic structures. *Adv. Mater.* **23**, 30–69 (2011).
18. C. M. Eliason, P.-P. Bitton, M. D. Shawkey, How hollow melanosomes affect iridescent colour production in birds. *Proc. Biol. Sci.* **280**, 20131505 (2013).
19. C. Nagasato, T. Motomura, Ultrastructural study on mitosis and cytokinesis in *Scytosiphon lomentaria* zygotes (Scytosiphonales, Phaeophyceae) by freeze-substitution. *Protoplasma* **219**, 140–149 (2002).
20. J. F. Galisteo-López, M. López-García, A. Blanco, C. López, Studying light propagation in self-assembled hybrid photonic–plasmonic crystals by fourier microscopy. *Langmuir* **28**, 9174–9179 (2012).
21. C. J. Chandler, B. D. Wilts, J. Brodie, S. Vignolini, Structural color in marine algae. *Adv. Opt. Mater.* **5**, 1600646 (2017).
22. S. Johnsen, E. A. Widder, The physical basis of transparency in biological tissue: Ultrastructure and the minimization of light scattering. *J. Theor. Biol.* **199**, 181–198 (1999).
23. H. Noh, S. F. Liew, V. Saranathan, S. G. J. Mochrie, R. O. Prum, E. R. Dufresne, H. Cao, How noniridescent colors are generated by quasi-ordered structures of bird feathers. *Adv. Mater.* **22**, 2871–2880 (2010).
24. J. F. Galisteo-López, E. Palacios-Lidón, E. Castillo-Martínez, C. López, Optical study of the pseudogap in thickness and orientation controlled artificial opals. *Phys. Rev. B* **68**, 115109 (2003).
25. S. Datta, C. T. Chan, K. M. Ho, C. M. Soukoulis, Effective dielectric constant of periodic composite structures. *Phys. Rev. B* **48**, 14936–14943 (1993).
26. P. S. M. Celis-Plá, N. Korbee, A. Gómez-Garreta, F. L. Figueroa, Seasonal photoacclimation patterns in the intertidal macroalga *Cystoseira tamariscifolia* (Ochrophyta). *Sci. Mar.* **78**, 377–388 (2014).
27. R. O. Prum, R. Torres, Structural colouration of avian skin: Convergent evolution of coherently scattering dermal collagen arrays. *J. Exp. Biol.* **206**, 2409–2429 (2003).
28. J. Sinclair, Y.-I. Park, W. S. Chow, J. M. Anderson, Target theory and the photoinactivation of photosystem II. *Photosynth. Res.* **50**, 33–40 (1996).
29. Y. I. Park, W. S. Chow, J. M. Anderson, Chloroplast movement in the shade plant Tradescantia albiflora helps protect photosystem II against light stress. *Plant Physiol.* **111**, 867–875 (1996).

30. A. L. Holt, S. Vahidinia, Y. L. Gagnon, D. E. Morse, A. M. Sweeney, Photosymbiotic giant clams are transformers of solar flux. *J. R. Soc. Interface* **11**, 20140678 (2014).
31. A. Mihi, M. E. Calvo, J. A. Anta, H. Miguez, Spectral response of opal-based dye-sensitized solar cells. *J. Phys. Chem. C* **112**, 13–17 (2008).

Acknowledgments: We would like to acknowledge M. Vos and C. Lowe from the University of Exeter in Falmouth for contacting us about the iridescence in *Cystoseira* and helping us locate samples. We would also like to acknowledge the assistance of J. Mantel and P. Verkade at the University of Bristol Wolfson Bioimaging Facility and Quorum Technologies for assistance with microscopy methods. **Funding:** We are grateful for funding from the European Research Council (project number 260920 to H.M.W.). M.L.-G. acknowledges funding from the Engineering and Physical Sciences Research Council (EPSRC) under grant EP/G004366/1, and J.L. was funded by EPSRC through grant number EP/M506473/1 and through a summer student bursary EP/M507994/1. **Author contributions:** M.L.-G., N.M., H.E.O., R.O., and H.M.W. conceived the experiments. M.L.-G., N.M., J.L., and G.A. carried out the optical analysis. M.L.-G. and R.O. designed and ran optical models. M.L.-G., N.M., H.E.O., M.J.C., J.L., and G.A. identified and collected the species in the field. H.E.O. and N.M. carried out the electron and confocal microscopy. M.L.-G., N.M., H.E.O., R.O., and H.M.W. wrote the manuscript, on which all authors commented. **Competing interests:** The authors declare that they have no competing interests. **Data and materials availability:** All data needed to evaluate the conclusions in the paper are present in the paper and/or the Supplementary Materials. Additional data related to this paper may be requested from the authors.

Submitted 14 May 2017
Accepted 22 February 2018
Published 11 April 2018
10.1126/sciadv.aan8917

Citation: M. Lopez-Garcia, N. Masters, H. E. O'Brien, J. Lennon, G. Atkinson, M. J. Cryan, R. Oulton, H. M. Whitney, Light-induced dynamic structural color by intracellular 3D photonic crystals in brown algae. *Sci. Adv.* **4**, eaan8917 (2018).

Science Advances

Light-induced dynamic structural color by intracellular 3D photonic crystals in brown algae

Martin Lopez-Garcia, Nathan Masters, Heath E. O'Brien, Joseph Lennon, George Atkinson, Martin J. Cryan, Ruth Oulton and Heather M. Whitney

Sci Adv **4** (4), eaan8917.
DOI: 10.1126/sciadv.aan8917